Ion beam oxidation

J. M. E. Harper, M. Heiblum, J. L. Speidell, and J. J. Cuomo
IBM Thomas J. Watson Research Center, Yorktown Heights, New York 10598

(Received 15 December 1980; accepted for publication 1 March 1981)

We describe a new technique for controlled oxide growth using a directed low-energy ion beam. The technique is evaluated by fabricating Ni-oxide-Ni and Cr-oxide-Ni tunneling junctions, using oxygen ion beams with energies ranging from 30 to 180 eV. High ion current densities are achieved at these low energies by replacing the conventional dual grid extraction system of the ion source with a single fine mesh grid. Junction resistance decreases with increasing ion energy, and oxidation time dependence shows a characteristic saturation, both consistent with a process of simultaneous oxidation and sputter etching, as in the rf oxidation process. In contrast with rf oxidized junctions, however, ion beam oxidized junctions contain less contamination by backsputtering, and the quantitative nature of ion beam techniques allows greater control over the growth process.

PACS numbers: 73.40.Rw, 68.55. + b, 79.20.Nc

Recent demands in the applications of metal-oxide-metal devices (MOM's) require very small areas and thin structures. In room-temperature applications, MOM's have been employed as infrared detectors and mixers up to the near infrared[1]. In cryogenic applications, MOM's are being used as Josephson junction switches in computer circuits and as detectors and mixers in the submillimeter range.[2] These devices require a uniform oxide thickness in the range 5–25 Å, which is difficult to achieve reproducibly using thermal or plasma oxidation. A process developed by Greiner,[3] combines simultaneous oxidation with sputter etching in an rf plasma to produce a steady-state, uniform oxide thickness. In this paper we describe a new process of controlled oxidation using a directed ion beam of well-defined energy and current density. The ion beam technique is compared with the rf process, and results are presented for oxidation of Ni and Cr using a low-energy oxygen beam.

The rf oxidation process is summarized as follows: Low-energy oxygen ions strike the metal with a broad energy spread[4]. Ions with kinetic energy less than the sputter threshold energy oxidize the metal, while ions with higher kinetic energy sputter etch the metal and oxide. If the initial oxide growth rate is higher than the sputter etching rate, the oxide thickness increases up to a steady-state value for which the oxidation rate equals the sputtering rate. By continuing the process longer than needed for having oxidation and sputtering rate equal, a pinhole free oxide is achieved with a reproducible final thickness.

Several drawbacks limit the usefulness of the rf oxidation technique. (1) Processing parameters are interdependent. Changing the pressure, for example, changes both the ion acceleration voltage and current density. (2) Energetic electron bombardment heats up the sample and hastens oxidation. (3) The plasma is at an elevated potential relative to the chamber walls, resulting in a constant sputtering of the walls. (4) Sputtered atoms scatter from the gas back onto the sample, contaminating the oxide. At a pressure of 10 mTorr (typically used in rf oxidation), the mean free path for back-sputtered neutrals is only a few mm, and it has been found, for example, that the current density of superconducting tunnel junctions is greatly affected by the presence of back-sputtered material.[5] The contamination problem is crucial when the potential barrier shape of the oxide has to be accurately known, as in hot-electron transfer amplifiers.[6]

The drawbacks of rf oxidation led us to develop a new process of ion beam oxidation using a large area, high current density oxygen ion beam with low energy. Broad beam multiaperture ion sources (Kaufman sources) are widely used for etching applications, and energetic ion beams have been used to carry out reactive processes in a variety of configurations.[7] Recently Kleinsasser *et al.*[8] reported the fabrication of Josephson junctions by ion beam oxidation of Nb, using an Ar/O_2 ion beam with energy of 600 eV. In this latter work, however, oxidation occurred rapidly and was not the result of combined oxide growth and sputter etching. To achieve this combined process we modified a Kaufman ion source to generate a high ion current density with ion energies below 100 eV, where a balance between oxide growth and sputter etching can be achieved. In a conventional Kaufman source,[9] ions are generated in a low-voltage, thermionically supported plasma inside a discharge chamber at a pressure of about 1 mTorr. Ions are extracted into a beam by an extraction region consisting of two thin grids with a dense pattern of aligned apertures. The beam is directed toward the sample situated in a low-pressure region of about 0.1 mTorr, and a neutralizer filament supplies electrons to compensate the positive charge of the ion beam.

The advantages of ion beam techniques include (1) independent control over ion beam energy and current density. (2) Samples are isolated from the ion generation plasma. (3) Chamber walls are not subjected to energetic ion bombardment, since the beam is directed. (4) Since the mean free path of ions and sputtered atoms is greater than the chamber dimensions, back sputtering is minimized. (5) Ions have a narrow energy spread (10-20 eV), enabling easier analysis. Although high current densities are produced at ion energies of several hundred eV, the conventional ion source with dual extraction grids is severely limited at low ion energy (< 100 eV) due to the space-charge-limited ion current between the grids[9]. (The maximum ion current is determined by the voltage difference between the grids, V_t, which is approximately equal to the ion beam energy.) For example, a dual grid sys-

 0021-8979/81/064118-04$01.10

tem which produces a maximum current density of 1 mA/cm^2 at $V_t = 500$ V will produce only 0.03 mA/cm^2 at $V_t = 50$ V. Since 1 mA/cm^2 corresponds to an ion flux of 6.5×10^{15} ion/cm^2 sec, and solid surface atom densities are about 10^{15} atom/cm^2, it is evident that a dual grid extraction system is incapable of producing oxides in short enough times to avoid contamination problems when low ion energies (hence low V_t) are used.

To maintain high current density at low ion energy, we use a single extraction grid[10] for which the ion current density is not space-charge limited, and current densties up to 1.0 mA/cm^2 are obtained at ion energies well below 100 eV.[11] This approach has recently been applied to reactive ion beam etching at low ion energy.[11]

The experimental configuration for ion beam oxidation is shown in Fig. 1. The sample to be oxidized is mounted with Ga-backing on a water cooled Mo-coated copper block. Samples were prepared by sputter coating Si wafers with 1000 Å of either Ni or Cr followed by a layer of 1000 Å of SiO_2. The SiO_2 was chemically etched to define junction areas ranging from 5 to 40 μm^2, in which the oxide was grown. A 7-cm-diam ion source equipped with a Ni mesh single grid of 100 line/inch faces the sample at a distance of 15 cm. This ion source performs both precleaning and oxidation of the sample. A movable shutter protects the sample, and a retarding grid energy analyzer can be moved into the beam path to measure the ion beam energy distribution and current density. A dual grid ion source directs a 2.0-cm-diam beam at a movable Ni target to overcoat the oxidized sample with a Ni counterelectrode.

Typical electrical parameters of the single grid ion source (Fig. 1) are as follows: i_c, cathode heater current of typically 13 A; V_d, discharge voltage needed to sustain the plasma, 40 V for Ar and 70 V for O_2; V_a, anode voltage approximately equal to the desired ion energy (20–150 eV); V_g, grid voltage ($-$ 10 V); i_n, neutralizer heater current of typically 6.5 A. The gas pressure in the sample chamber is 0.3 mTorr. The dual grid ion source was operated to produce an 800-eV, 12-mA Ar^+ ion beam for a deposition rate of nickel of about 2 Å/sec.

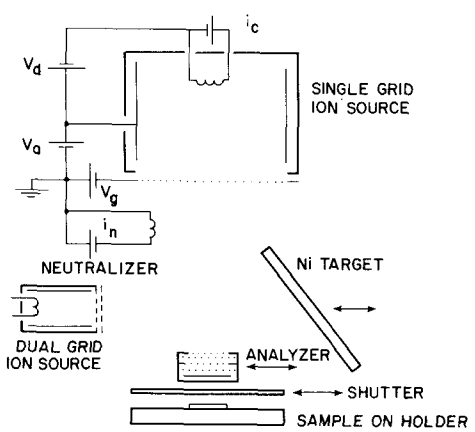

FIG. 1. Schematic diagram of ion beam oxidation system, showing single grid ion source for sputter cleaning and oxidation, dual grid ion source for overcoating of junctions, movable ion energy analyzer, and sample on water cooled holder.

After pumping the sample chamber to about 5×10^{-7} Torr, the Ni target is presuttered for 10 min with 800-eV Ar^+ ions. The sample is then sputter etched for 5 min using Ar^+ ions at 150 eV and 0.72 mA/cm^2 to remove several hundred Å of Ni. Argon is next replaced with oxygen and the beam adjusted to desired conditions using the analyzer. The sample is then oxidized with the low-energy oxygen ion beam. The Ni target is resputtered with Ar^+ for 5 min (with the sample protected) to remove any oxide formed on the target during oxidation, followed by overcoating of the sample with 500–1000 Å of Ni. Up to six samples may be oxidized and overcoated independently in one run. Samples are then removed from the vacuum system and top electrodes are patterned and chemically etched above the oxidized areas as shown in Fig. 2(a).

To evaluate the process of ion beam oxidation, nickel and chromium metal films were oxidized by oxygen ion beams with energy ranging from 30 to 180 eV and current density of 0.72 mA/cm^2 for times ranging from 10 sec to 30 min. To compare with MOM's prepared by the rf oxidation technique, additional samples were processed using a feedback controlled rf diode sputtering system.[12] Nickel elec-

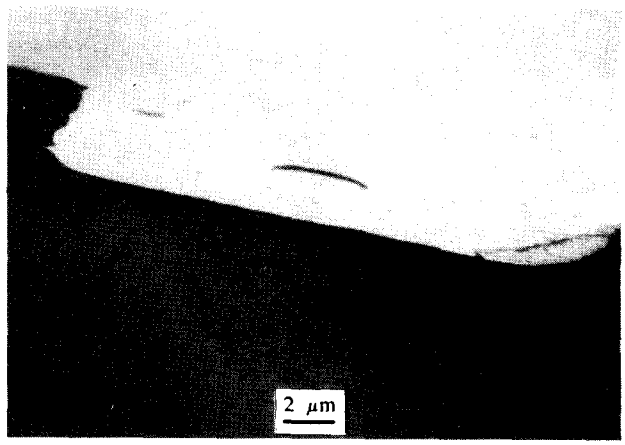

(a)

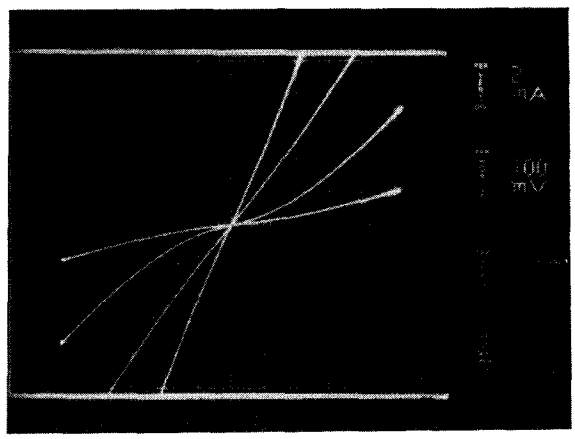

(b)

FIG. 2. (a) SEM picture of metal-oxide-metal junction (circular area). The light region is the top Ni electrode, and the dark region is the SiO_2 masking layer over the bottom electrode (Taken at 70° from normal to substrate). (b) Current-voltage characteristics of Ni-NiO-Ni MOM's produced by ion beam oxidation. Junction resistances range from over 10 kΩ (lowest slope curve) to less than 25 Ω (steepest curve), as ion energy is increased from 30 to over 100 eV. Oxidation dose is 0.72 mA/cm^2 for 10 min.

trodes of 10-μm^2 area were rf oxidized for 30 min using substrate electrode voltages ranging from 5 to 50 V (dc value), at 20-mTorr oxygen pressure and power levels of approximately 10 mW/cm^2. Overcoating was carried out by rf sputtering a nickel target, followed by patterning of the junction top electrodes.

For each junction, the dynamic resistance was measured at zero bias as an indicator of oxide thickness. To indicate the range of values obtainable, current-voltage curves are shown in Fig. 2(b) for nickel-oxide-nickel junctions fabricated by ion beam oxidation. For low oxygen ion energy (30–40 eV), junction resistances of 10 kΩ or higher are obtained after several minutes oxidation [the curve of lowest slope in Fig. 2(b)]. By increasing oxygen ion energy, the junction resistance decreases to as low as 25 Ω for energies above 100 eV [the curve of highest slope in Fig. 2(b)]. Junctions are stable under biasing, with breakdown voltages of 1.5–2.5 V at room temperature (lead resistance is 20 Ω). Increasing ion beam energies to above 150 eV results in shorted junctions.

The dependence of junction resistance (10-μm^2 area) on oxygen ion beam energy is shown in Fig. 3, for both nickel and chromium junctions oxidized for 10 min at oxygen ion current density of 0.72 mA/cm^2. The spread of ion energy in the beam (typically 20 eV) is shown for each point[13]. As indicated in Fig. 2(b), junction resistance of nickel and chromium MOM's decreases with increasing oxygen ion beam energy, presumably due to increased sputter etching. Chromium MOM's have somewhat higher resistances due to the greater reactivity of chromium.

For comparison, the dependence of junction resistance on maximum oxygen ion energy is also shown in Fig. 3 for 10-μm^2 Ni-NiO-Ni rf oxidized junctions. Here, the maximum ion energy is determined by the sum of the self-generated dc cathode voltage and the plasma potential (typically + 20 V), and the energy spread is known to extend continuously to zero, due to charge exchange collisions[4]. The energy dependences of junction resistance for the rf oxidized and ion beam oxidized MOM's are similar, which suggests that a combined sputter-oxidation process is relevant in both cases.

Time dependence of junction resistance was also examined for ion beam oxidized Ni junctions (Fig. 4). At an oxygen ion energy of 45 eV, the nickel junction resistance increases monotonically with oxidation time, indicating an oxide growth component with negligible sputter etching. For an oxygen ion energy of 80 eV, however, the junction resistance saturates after several minutes, indicating the formation of a steady-state oxide thickness.

Some parameters governing the oxide growth can be deduced from Fig. 4. We assume that the junction tunneling resistance at low bias voltage is given by $R(x) = Ax \exp(Bx)$, where R is the dynamic resistance at zero bias, x is thickness, and A and B are constants[14]. For a barrier height of 1 eV, an oxide thickness of 12.5 Å leads to a resistance of 1.5 kΩ for a 10-μm^2 junction area. We now assume that the oxide growth rate is given by an exponentially decreasing function of thickness in combination with a constant sputter etching rate $dx/dt = K \exp(-x/X_0) - E$, where K is the initial oxidation rate in the absence of sputtering, X_0 is a constant determined by the rate of oxygen diffusion through the oxide, and E is the sputter etching rate.[3] In the presence of sputtering, the final oxide thickness is $X_0 \ln(K/E)$, which is approached with a time constant X_0/E. From the data for an ion energy of 80 eV (Fig. 4), we estimate a time constant of about 1 min. Assuming a sputtering rate of about 2 Å/min for nickel oxide under 80 eV O_2^+ bombardment at 0.72 mA/cm^2, we get $X_0 = 2$ Å. Since $K \gg 1$ (measured to be about 10^3 Å/min. for PbIn-oxide[15]), $x(t) = X_0 \ln[(K/X_0)t]$ for time scales used in our measurements in the absence of sputter etching. We now express the junction resistance as a function of time: $\ln R = C + BX_0 \ln t$, where $C = \ln A + \ln x + BX_0 \ln(K/X_0)$. C can be regarded as a con-

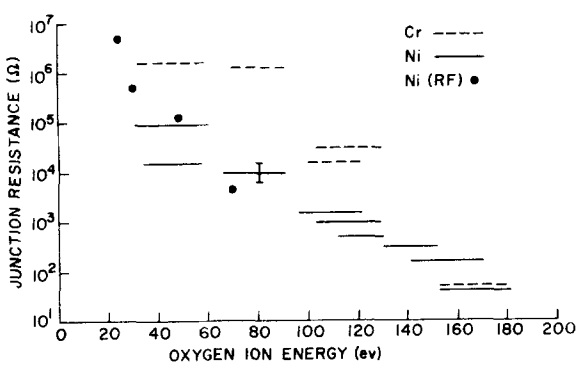

FIG. 3. MOM junction resistance (normalized to 10-μm^2 area) vs oxygen ion energy. Solid lines are for Ni junctions, ion beam oxidized for 10 min at 0.72 mA/cm^2. The width of each line is the ion energy spread. Dashed lines are for Cr junctions oxidized by the same dose. Dots are for Ni junctions, rf oxidized for 30 min.

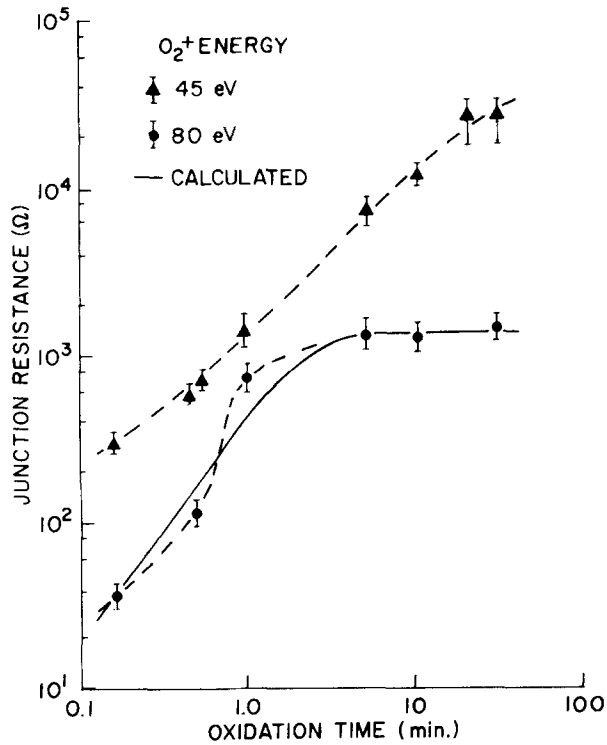

FIG. 4. MOM junction resistance (normalized to 10-μm^2 area) vs ion beam oxidation time. Triangles are for 45-eV and dots are for 80-eV oxygen ion energies. Current density is 0.72 mA/cm^2. The solid line is the calculated time dependence of junction reisitance (including 20-Ω lead resistance).

stant due to weak dependence of $\ln x$ on t. The linear dependence of $\ln R$ on $\ln t$ is qualitatively seen in the 45-eV curve of Fig. 4.

From the final resistance of 1.5 kΩ, one gets $K \cong 1000$ Å/min. This value of initial oxidation rate is reasonable since the arrival rate of oxygen ions at 0.72 mA/cm^2 corresponds to approximately one monolayer of oxygen per second. If each ion were incorporated in the oxide, the growth rate would be several hundred Å/min. (Note that different estimates of the time constants or the etching rate will change X_0 and K. Round numbers are chosen for convenience.) Substituting X_0, E, and K in $x(t)$ for the general case of sputter oxidation[3,15] leads to $x(t) \cong 2 \ln 500[1 - \exp(-t)]$. Using the equation for $R(x)$, the resistance is plotted in Fig. 4 with a fairly good agreement with the measured resistances (lead resistance of 20 Ω is added). The results strongly suggest that a combined oxidation and sputtering process is responsible for the observed time dependence of junction resistances.

The detailed mechanism of rf oxidation is not yet understood, and several processes have been proposed to account for the enhanced oxidation which is generally observed in the rf oxidation process[15,16]. While our present results do not allow us to comment in detail on these models, we have used the directed nature of ion beams to limit the possible species which are necessary for ion beam oxidation. Generally, a variety of species bombards the sample: (1) energetic oxygen ions accelerated from the ion source, (2) thermal neutral oxygen molecules, (3) thermal oxygen atoms formed by dissociation in the discharge, (4) energetic oxygen neutrals formed by charge exchange between beam ions and background neutrals, (5) low-energy (several eV) electrons from the beam plasma. By masking the sample with a shutter during oxidation, allowing only background neutrals to reach the sample, shorted devices were obtained, indicating that thermal oxidation is negligble. Several samples were processed using a deflecting mesh to remove all positive ions from the beam, allowing only electrons, thermal neutrals, and energetic neutrals to reach the sample. Energetic charge exchange neutrals might represent about 10% of the total ion flux at the existing pressure of 3×10^{-4} Torr.[17] In a series of deflection experiments carried out with ion energies of 40, 70, and 100 eV, we observed some oxidation even in the absence of ions. We reach the preliminary conclusion that ion beam oxidation is carried out by energetic ions and energetic charge exchange neutrals in the beam. The roles of low-energy electrons and thermal monatomic oxygen are still not established.

To further characterize the oxidation processes, Auger spectra were taken on both rf and ion beam oxidized Ni and Cr samples (after air transfer). In all samples, 40–60% carbon contamination was detected, probably due to the air transfer and the exposure to diffusion pump vapor. In rf oxidized samples, large amounts (6–17%) of molybdenum, backsputtered from the sample holder, were observed in addition to the Ni, Cr, and O in the oxide. By contrast, Mo was not detected in ion beam oxidized films, indicating one of the advantages of operating at low pressure. In ion beam oxidized Cr samples, trace amounts ($< 1\%$) of Ni were found, probably sputtered from the Ni single grid mesh.

We have demonstrated a new process of metal oxidation which incorporates the advantages of low-energy ion beams. The process is easily controlled and reproducible, and the resulting oxide junctions are of high quality and free of the contaminants usually found in the rf oxidation process. We expect that the flexibility of ion beam systems with regard to physical configuration and electrical control will lead to further clarification of the oxidation mechanisms.

ACKNOWLEDGMENTS

We thank G. A. Waters, D. L. Goldman, and G. M. Summa for helping to develop the ion oxidation process. We also thank R. Ludeke and G. Landgren for carrying out Auger analysis and L. Osterling for assistance in lithography. We thank J. M. Baker for discussion of his results prior to publication.

[1] Recent results and references can be found in M. Heiblum, S. Y. Wang, T. K. Gustafson, and J. R. Whinnery, J. Quantum Electron. **QE-14**, 159 (1978); M. Heiblum, Ph.D. thesis, University of California, Berkeley, 1978 (unpublished).
[2] C. A. Hamilton, Cryogenics **20**, 235 (1980).
[3] J. H. Greiner, J. Appl. Phys. **42**, 5151 (1971); **45**, 32 (1974).
[4] L. I. Maissel and R. Glang, *Handbook of Thin Film Technology* (McGraw-Hill, New York, 1970), Chaps. 3–44.
[5] J. M. Baker, C. J. Kircher, and J. W. Matthews, IBM J. Res. Develop. **24**, 223 (1980); J. M. Baker, Eighth International Vacuum Congress, Sept. 1980, Cannes, France (unpublished).
[6] M. Heiblum, Solid State Electronics, April 1981.
[7] C. Weissmantel, Thin Solid Films **32**, 11 (1976); J. A. Taylor, G. M. Lancanster, A. Ignatiev, and J. W. Rabalais, J. Chem Phys. **68**, 1776 (1978).
[8] A. W. Kleinsasser and R. A. Buhrman, *Proceedings of Ninth International Conference on Electron and Ion Beam Science and Technology*, St. Louis, Mo. 1980 Vol. 80-6 (Electrochem. Soc. Pennington, NJ, 1980).
[9] H. R. Kaufman, J. Vac. Sci. Technol. **15**, 272 (1978).
[10] P. LeVaguerese and D. Pigache, Rev. Phys. Appl. **6**, 325 (1971).
[11] J. M. E. Harper, J. J. Cuomo, P. A. Leary, G. M. Summa, H. R. Kaufman, and F. R. Bresnock, J. Electrochem. Soc. May 1981.
[12] A. Halperin, P. Silano, and L. West, J. Vac. Sci. Technol. **15**, 116 (1978).
[13] The values of energy spread at ion energies above 100 eV may not be reliable since the analyzer readings are distorted by space charge at a high current density range.
[14] J. G. Simmons, J. Appl. Phys. **34**, 1793 (1963). The constants in the equation are $A = (\hbar^2/e^2)(1/2m^*\phi)^{1/2}$, $B = [(4\pi)^2 2m^*\phi/h^2]^{1/2}$, where ϕ is the barrier height and m^* is the effective mass of the electron, which we assume here to be m_0.
[15] P. C. Karulkar and J. E. Nordman, J. Appl. Phys. **50**, 7051 (1979).
[16] A. T. Fromhold and J. M. Baker, J. Appl. Phys. **51**, 6377 (1980).
[17] R. S. Robinson, J. Vac. Sci. Technol. **16**, 185 (1979).